Title
Geometry of Geyser Plumbing Inferred From Ground Deformation

Journal
Journal of Geophysical Research: Solid Earth, 124(1)

ISSN
2169-9313

Authors
Ardid, Alberto
Vera, Emilio
Kelly, Cyndi
et al.

Publication Date
2019

DOI
10.1029/2018jb016454

Peer reviewed

Geometry of Geyser Plumbing Inferred From Ground Deformation

Alberto Ardid[1,2], Emilio Vera[1,2], Cyndi Kelly[3], Michael Manga[4], Carolina Munoz-Saez[2], Andrei Maksymowicz[1], and Francisco Ortega-Culaciati[1,5]

[1] Departamento de Geofísica, Facultad de Ciencias Físicas y Matemáticas, Universidad de Chile, Santiago, Chile, [2] Andean Geothermal Center of Excellence (CEGA), Facultad de Ciencias Físicas y Matemáticas, Universidad de Chile, Santiago, Chile, [3] Department of Geophysics, Stanford University, Stanford, CA, USA, [4] Department of Earth and Planetary Science, University of California, Berkeley, CA, USA, [5] Advanced Mining Technology Center, Facultad de Ciencias Físicas y Matemáticas, Universidad de Chile, Santiago, Chile

Correspondence to: A. Ardid, aardids@gmail.com

Abstract

Broadband seismic data were recorded on the ground surface around an exceptionally regular eruptive system, geyser *El Jefe*, in the El Tatio geyser field, Chile. We identify two stages in the eruption, recharge and discharge, characterized by a radial expansion and contraction, respectively, of the surface around the geyser. We model the deformation with spherical sources that vary in size, location, and pressure, constrained by pressure observations inside the conduit that are highly correlated with deformation signals. We find that in order to fit the data, the subsurface pressure sources must be laterally offset from the geyser vent during the recharge phase and that they must migrate upward toward the vent during the eruption phase. This pattern is consistent with models in which ascending fluids accumulate and then are released from a bubble trap that is horizontally offset from the shallow conduit of the geyser.

1 Introduction

Geysers are rare phenomena: they require a hot water supply and subsurface structures that allow the circulation of fluids (water, steam, and noncondensable gases) in a manner that leads to noncontinuous eruption. Geysers are thus sometimes viewed as curiosities. However, their existence raises an important question and opportunity. What subsurface structures are required to produce geysers? And, while geyser eruptions are smaller and more frequent than those produced at magmatic volcanoes, they also provide an opportunity to test approaches for measuring and modeling geophysical signals in eruptive systems (Kieffer, 1984; National Academies, 2017).

Geophysical methods have been used to image spatial and temporal variations in the subsurface properties of geysers, complementing pressure, temperature, and audiovisual measurements. For example, Kedar et al. (1996, 1998) showed that hydrothermal tremor at Old Faithful Geyser in Yellowstone National Park is produced by collapsing steam bubbles. From

this same data set, Cros et al. (2011) and Vandemeulebrouck et al. (2013) used ambient noise processing techniques to reveal a deeper cavity that is laterally offset from the conduit below the surface vent, as proposed more than two centuries ago by Mackenzie (1811). Nishimura et al. (2006) used tilt observations at Onikobe geyser, NE Japan, to show a strong correlation with the short and long effusion times, reflecting water movement in at least two chambers beneath the vent. From tilt measurements at Old Faithful Geyser of Calistoga, California, Rudolph et al. (2012) showed that surface ground deformations record the gradual filling and rapid emptying of reservoirs. These studies show how seismic and geodetic measurements over a range of frequencies can be used to characterize the plumbing systems of, and pressures within, geysers. Additional imaging tools include using microphones (e.g., Namiki et al., 2016), forward looking infrared (e.g., Karlstrom et al., 2013), and ground-penetrating radar to characterize the shallowest subsurface (e.g., Lynne et al., 2017, 2018).

Geophysical techniques are needed because the plumbing systems of some geysers are difficult to image directly, though video cameras have imaged at least parts of the main conduits beneath geysers (e.g., Yellowstone: Hutchinson, 1985, Hutchinson et al., 1997; Kamchatka: Belousov et al., 2013; Iceland: Walter et al., 2018). Subsurface geometry matters because large and deep cavities may control the size and frequency of eruptions (e.g., Adelstein et al., 2014; Hurwitz & Manga, 2017). Further support for a deep control on eruptive processes is the insensitivity of eruptions at cone geysers to changes in atmospheric pressure and temperature (e.g., Hurwitz et al., 2014; Munoz-Saez, Namiki, & Manga, 2015).

All these studies have contributed significantly to improving our understanding of the special conditions needed to produce geysers. However, the temporal evolution of physical processes that govern eruptions and their connection to the geometry of plumbing systems remain poorly documented. During the eruptive cycle, spatial and temporal variations in pressure at depth depend on the geometry of the plumbing system. Ground surface deformation produced by those changes in pressure offers an opportunity to better constrain the subsurface processes that accompany geyser eruptions.

Here we use passive broadband seismic data acquired around *El Jefe* geyser at the El Tatio geyser field, Chile, to model the space-time variation of subsurface pressure conditions over the course of an eruption cycle, constrained by conduit pressure measurements (Munoz-Saez, Manga, et al., 2015).

2 El Tatio Geyser Field

El Tatio geyser field is located in the Atacama desert of northern Chile (Figure 1a). Here more than 200 thermal features (Glennon & Pfaff, 2003) discharge regionally derived meteoric water (e.g., Munoz-Saez et al., 2018) mixed with magmatic fluids (e.g., Tassi et al., 2010). Of the thermal features,

about 80 are geysers that erupt periodically or episodically at the local boiling temperature of water (86.6 °C).

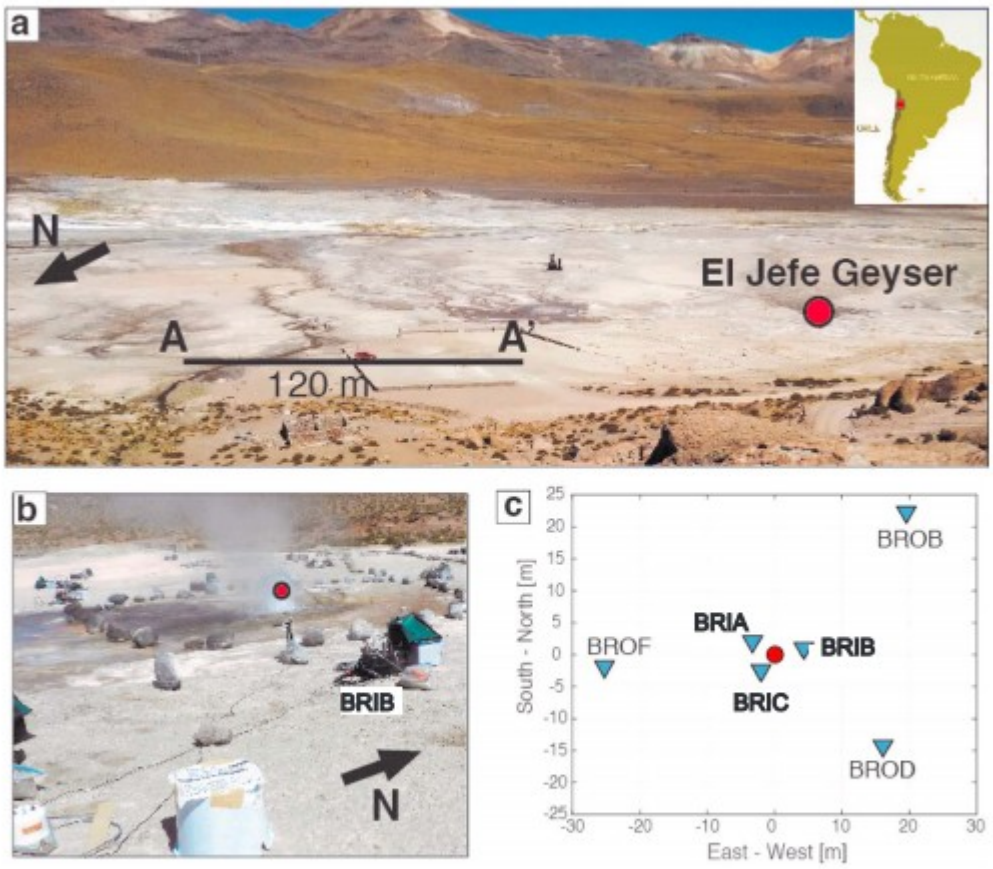

Figure 1. (a) Photograph of the Upper Geyser Basin of the El Tatio Geyser Field; El Jefe geyser (UTM coordinates 601768°E, 7530174°S, WGS84-19S) is marked by the red dot. The active seismic profile (AA′) is shown. (b) El Jefe geyser erupting. (c) Broadband network around El Jefe geyser (red circle; E601,768; 7,530,174°S, WGS84-19S). The blue triangles show the locations of the stations.

The basins containing the geysers are filled with Miocene ignimbrites, andesitic volcanic agglomerates, and Plio-Holocene dacitic and rhyolitic ignimbrites, and lavas (Marinovic & Lahsen, 1984). Glacial and alluvial deposits, and locally derived silica sinter deposits from the geysers, define the shallowest geology (e.g., Fernandez-Turiel et al., 2005; Marinovic & Lahsen, 1984; Munoz-Saez et al., 2016; Nicolau et al., 2014). Permeable ignimbrites host the geothermal reservoir feeding the geysers, which are underlain by low permeability andesitic rocks and capped by low permeability silica sinter deposits (Cusicanqui et al., 1975; Giggenbach, 1978).

El Jefe geyser is located in the Upper Geyser Basin of the El Tatio Geyser Field (Figure 1a). During a monitoring experiment in 2012 (Munoz-Saez, Namiki, & Manga, 2015), this geyser exhibited a regular eruption interval of 132 ± 2 s. Although El Jefe is one of the smallest geysers in the basin, it

nevertheless produces detectable ground surface deformations that are coherent between stations deployed around the geyser.

3 Passive Seismic Experiment Data

We performed a passive seismic experiment around El Jefe geyser to document ground deformation before, during, and after eruptions. From 22–27 October 2012, we deployed six broadband seismometers (Trillium 120) on the surface around El Jefe geyser (Figure 1c). Three were located within about 3 m of the geyser, defining an inner network (BRIA, BRIB, and BRIC). The other three sensors (BROF, BROB, and BROD) were located farther from the geyser, about 15-m distant, forming an outer network. The sensors recorded three components of ground velocity at 500 Hz.

We also performed an active seismic experiment to estimate elastic properties for high-frequency deformation of the rocks that host the geysers. Details can be found in Supplement S2. We employed the Johnson (1976) formulation of split-spread refraction data to map plane dipping layers and construct the velocity model for the *P* wave and *SH* waves.

From the passive experiment, Figure 2 shows velocity signals at stations BRIA, BRIB, and BRIC. As it can be appreciated the temporal changes of the vertical component during the geyser's cycle are much smaller than the changes of the horizontal ones suggesting the presence of tilt (static component of horizontal rotations) in the signals. Given that the stations are located in the very near field, just a few meters from the source, the rotation could dominate over ground translations, as these sensors are also sensitive to rotations and the output signal will be a combined mixture of translations and rotations (Pillet & Virieux, 2007). The predominance of rotations over displacements in the low-period seismic signal has been considered at volcanoes (e.g., Genco & Ripepe, 2010; Lyons et al., 2012; Maeda & Takeo, 2011; Sanderson et al., 2010; Waite et al., 2013), as well as near geysers (Vandemeulebrouck et al., 2014) to model the ground deformation in the near field. Tilt signals are removed in the frequency domain as the tilt component can be calculated from the motion relative to ground acceleration. More details can be found in Supplement S1.

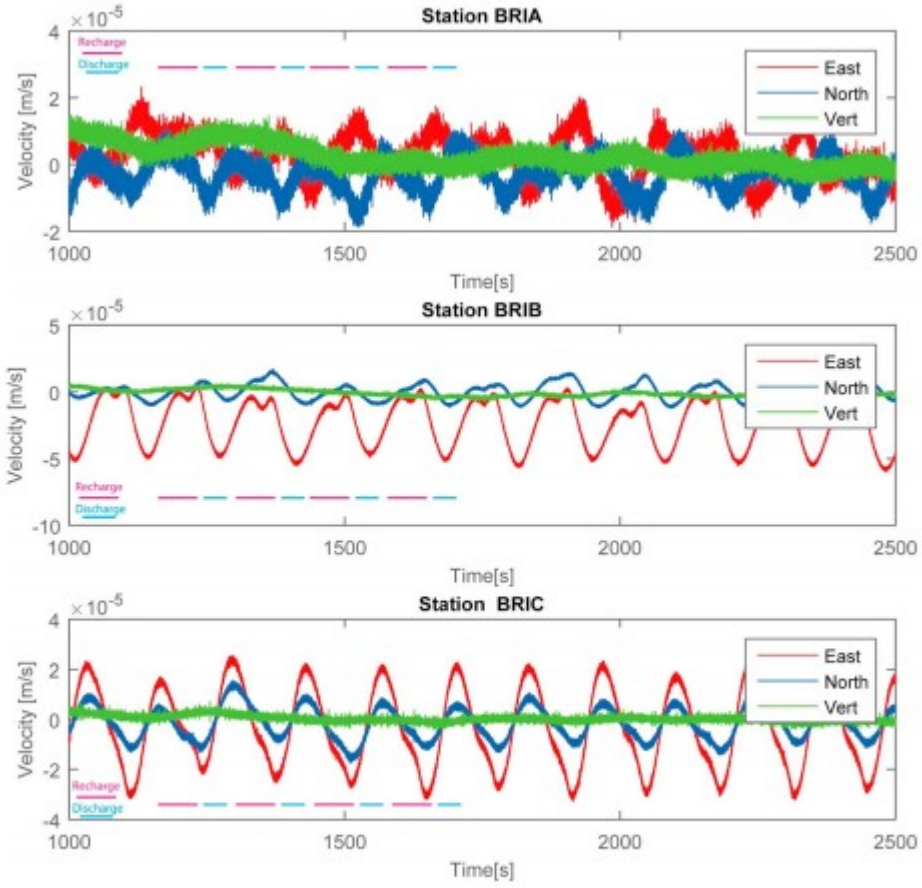

Figure 2. Velocity records at stations BRIA, BRIB, and BRIC in their three components: east (red), north (blue), and vertical (green). Signals recorded between 21:00 and 22:00 on 22 October 2012.

Figure 2 also shows how the inner network stations recorded a characteristic period of 132 s. Figure 3b shows the horizontal ground displacement (east-west component) at the BRIB and BRIC stations. The signals have a dominant periodicity of around 132 s, reflecting the periodicity of the El Jefe eruptive cycle in 2012 (also noted in Munoz-Saez, Namiki, & Manga, 2015). For the external network, other periods are superimposed on the 132-s period, presumably signals from the other geysers in the area, some of which are much larger than El Jefe (see Figures S1.5–S1.7). In addition, the single-sided amplitude spectrum for the stations of the inner network (see Supplement S1 and Figure S1.9) verifies the dominance of this characteristic period of 132 s.

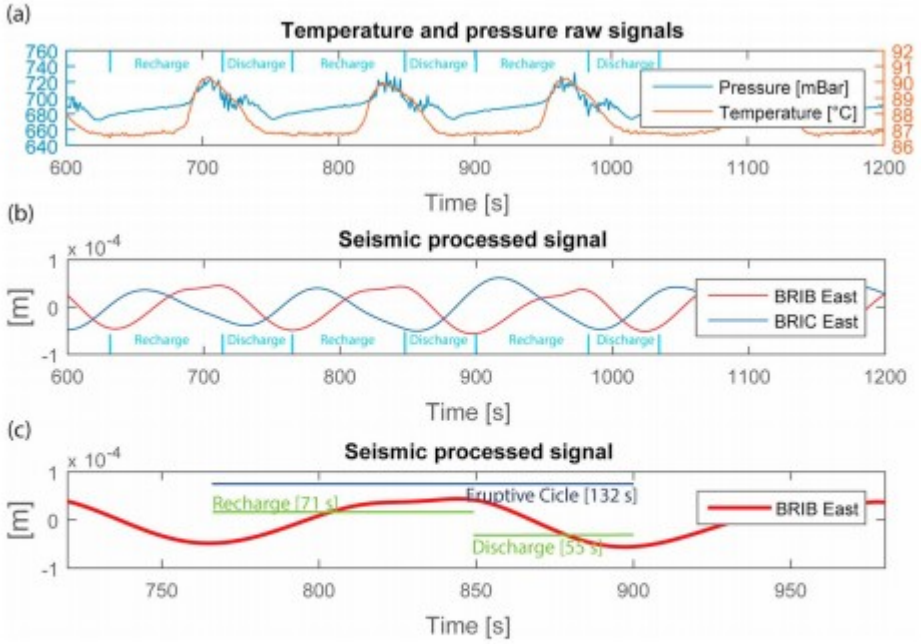

Figure 3. (a) Pressure and temperature recorded at a depth of 1.5 m inside El Jefe (from Munoz-Saez, Manga, et al., 2015). (b) Processed long-period displacement (see Supplement S1 for the equivalent raw and processed signals for the whole network and details of the data processing). (c) Displacement during one eruption cycle. (a and b) Signals were recorded over the same time period (signals recorded between 21:10 and 22:20 on 22 October 2012).

Figure 3c shows an eruptive cycle at the BRIB East station. The cycle is divided into two stages: recharge and discharge, with the former being longer. This pattern is clearly seen in the horizontal motion of the internal network. As can be seen in Figure 3b, the direction of horizontal movement at the BRIB and BRIC stations (located on opposite sides of the geyser) is antisymmetric. This is observed at the three stations of the internal network in their two horizontal components (see Supplement S1). These antisymmetric movements occur with respect to a central point close to the vent of the geyser.

Figure 3a shows the pressure and temperature recorded at a depth of 1.5 m within El Jefe (data from Munoz-Saez, Manga, et al., 2015). These signals were recorded at the same time as the seismic records shown in Figure 3b. Figure S1.11 shows a correlation analysis between the pressure signal and broadband seismic signal of station BRIB east component in acceleration, velocity, and displacement, and a high coherency is observed at the expected periods (eruption interval). Overall, Figure 3 shows how the recharge stage (see the first panel, between ~225 and 325 s) is associated with an increase in pressure at 1.5-m depth, whereas pressure decreases during the discharge stage.

We calculate the interval between eruptions from station BRIC for 3 days of measurement (~1,500 samples) and obtain a mean of 132.2 ± 3.5 s. This period is identical to that recorded visually and with downhole pressure and temperature sensors (Munoz-Saez, Namiki, & Manga, 2015; see Figure 3a).

Within each cycle, we identify two stages in the eruption (Figure 3c): stage 1, recharge, and stage 2, discharge. Stage 1 has a longer duration and involves displacement in the direction away from the geyser, so the recharge stage is characterized by a radial expansion of the surface around the geyser. Stage 2 is shorter and produces displacement in a direction toward the geyser, so, the discharge stage is characterized by radial contraction with respect to the position of the geyser.

4 Modeling Ground Deformation

Our objective is to determine the properties of the sources that give rise to the observed surface deformation and how these sources change over time. We do so at discrete and equally spaced instants in time by searching the parameter space for a combination of size, location, and pressure change that best explains the measurements.

There are several steps in the data analysis. First, we process the seismograms to isolate the characteristic period of about 132 s in displacement. This involves deconvolution, removal of tilt effects (Genco & Ripepe, 2010; Rodgers, 1968; Sanderson et al., 2010), and integration and filtering of the signals (details in Supplement S1). To model the observations, we fit measured displacement to a spherical source in a homogeneous elastic half-space subject to changes in internal pressure (McTigue, 1987). We apply the model equations in a quasi-static manner by estimating the best solution at each instant in the displacement time series. We adjust five parameters in the McTigue (1987) model: spatial position (x, y, z) of the center of the spherical cavity, its radius (a), and the pressure change (p) in the cavity (see Figure S3.1 and Table S3.1).

Synthetic displacements are calculated using all possible combinations of the model parameters in a certain range (grid search). For each combination, we compare predicted surface displacements with filtered data and chose a combination of model parameters that minimizes the least squares misfit. We repeat the procedure on a grid of smaller ranges around the best solution in order to improve the precision of the results. We fit 150 and 50 windows of data equally spaced over 300 s and hence obtain a solution every 2 and 6 s, respectively. Model parameters are estimated independently for each time step, ignoring a potential correlation between model parameters at adjacent time steps.

The expanding and contracting region could be a cavity (Steinberg et al., 1981) or a porous medium (Ingebritsen & Rojstaczer, 1993), and our data cannot distinguish between these two possibilities. Mackenzie (1811) suggested that the geyser plumbing system consists of a large subterranean cavity connected to the ground surface by a conduit with the configuration of an inverted siphon. The cavity works as a trap for steam bubbles rising from below; it has an impermeable roof and gradually accumulates pressurized steam that periodically erupts through the water-filled conduit. For the modeling, in this study we thus assume that the deformation is caused by

pressure changes in the subsurface conduit system. We model the ground surface displacement with spherical sources that vary in size, location, and pressure, immersed in an elastic half-space, employing the McTigue (1987) equations. We require that the radius of the cavity cannot be greater than the depth. This physical constraint prevents solutions that extend above the surface. Therefore, we search under the condition that depth > radius.

In an effort to constrain the model with the pressure signals recorded in the conduit (see Figure 2), we take into account a mechanical model for internal oscillations in geysers with *bubble trap* configurations developed in Rudolph and Sohn (2017) in which ascending fluids are trapped beneath the roof of a cavity that is laterally offset from the eruption conduit. Hydraulic coupling between a bubble trap and the eruption conduit is also explored by Vandemeulebrouck et al. (2014). In a static system, the gas phase in a bubble trap is loaded by the fluids in the eruption conduit. In El Jefe geyser, from the changes in pressure observed at a depth of 1.5 m (from Munoz-Saez, Manga, et al., 2015; see Figure 3), the amplitude of the water level changes over a complete cycle is around 50 mbar or ~50 cm (liquid water column). We use this value to constrain the shear modulus in the McTigue equations, as this parameter jointly with pressure controls displacement magnitudes. Figure S3.10 shows the relationship between shear modulus and the magnitude of implied pressure changes; for a pressure change of 50 mbar, a shear modulus of 0.5×10^6 Pa is required to obtain displacement on the order of the observed 1 mm (see Figure 3).

We estimate the deformation source at different time points independently, ignoring temporal correlations in the behavior of the system. Each of the solutions over more than two eruption cycles has five optimal parameters. The set of optimal solutions for all times defines the general solution of the problem (Figures 4 and 5). We find a concentration of shallow solutions around 3 m in depth with radii of about 1 m primarily associated with stage 1 and deeper solutions concentrating around 10 m in depth with radii about 3 m associated with stage 2. Figure 5 shows the evolution of the source parameters over the two eruption cycles.

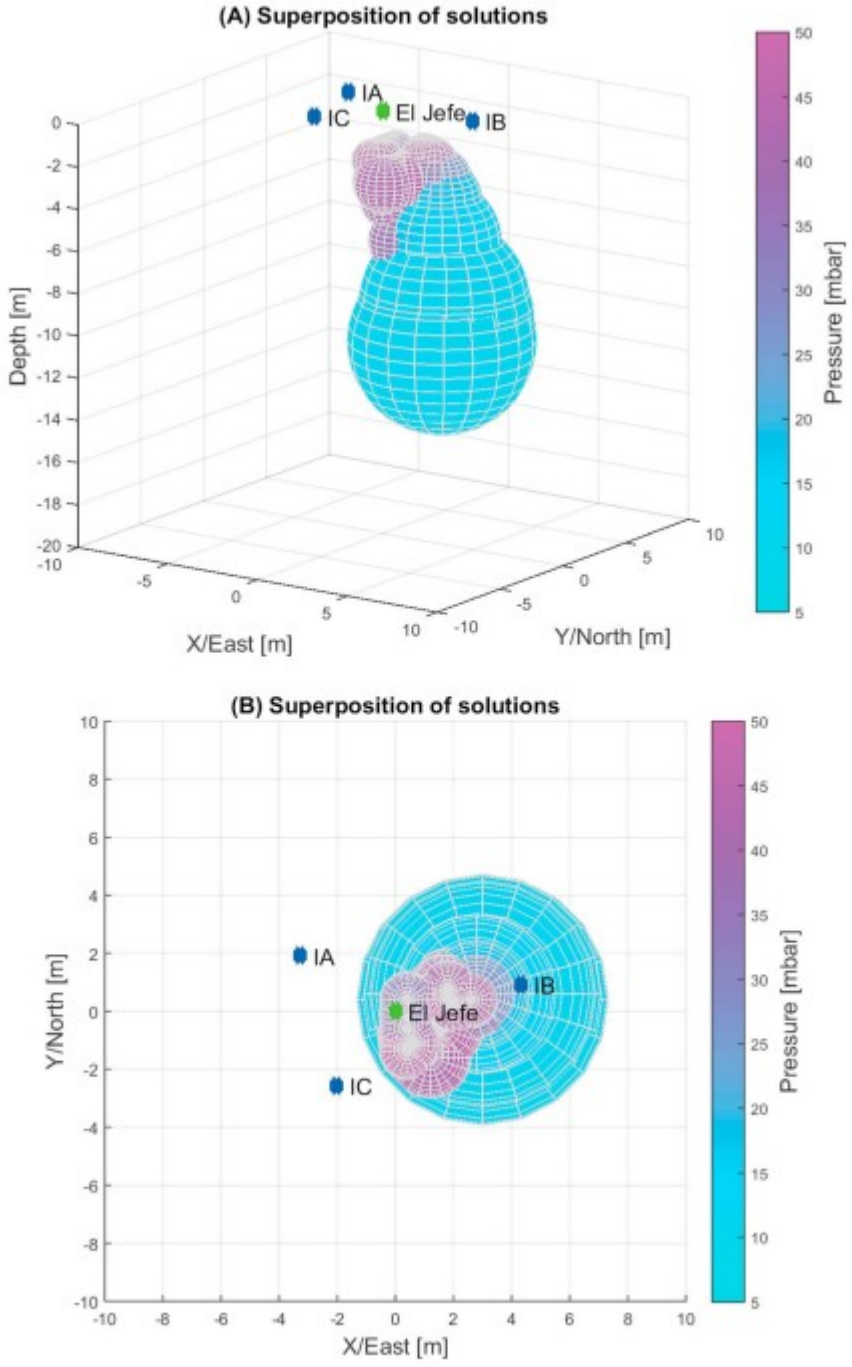

Figure 4. Optimal solutions for 2 cycles plotted every 2 s. (a) Side view (b) and map view. The blue dots show stations, and the green dot is the geyser vent. For details of the solutions, see Supplement S3.

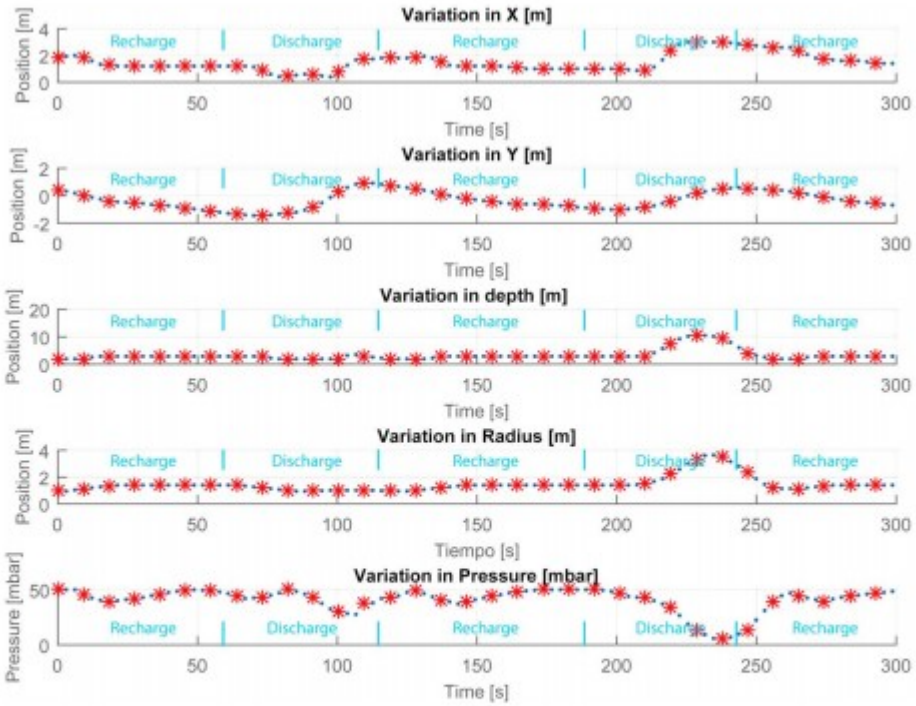

Figure 5. Variation of the optimal parameters covering 300 s. The cyclicity in all parameters is apparent. The best models fit well the large-amplitude horizontal displacements at the inner stations but not the vertical displacements nor the displacements at the distant stations. The blue dots are parameters estimated every 2 s, and the red asterisks are the ones estimated every 6 s. The models shown in Figure 4 are plotted directly from these parameters.

There are a number limitations in our analysis. First, we assume a homogeneous and isotropic medium when applying the deformation model. Second, we assume that the sources are spherical. This was done to minimize the number of parameters but is an idealization for what we know is a more complex plumbing system. Indeed, geyser conduits and cavities can be crack-like and tube-like (e.g., Hutchinson, 1985; Walter et al., 2018), though large cavities such as those we model may exist (e.g., Belousov et al., 2013; Vandemeulebrouck et al., 2013). We estimated the same order of magnitude (~1 mm) of surface deformation by a prolate spheroid (Fialko & Simons, 2000; vertically oriented, semiaxes 4 and 1 m) simulating a vertical conduit. This geometry considers half of the volume compared to spherical one, submitted to the same differential pressure, suggesting that the spherical assumption requires larger volumes for the source. Both assumptions may explain why we do not simultaneously fit horizontal and vertical displacements (see Figure 6). Third, the use of a grid search to identify model parameters is not computationally efficient. Fourth, by minimizing the global error (all stations), the model is biased to the stations that have the largest displacements, thus prioritizing data from the internal network. However, this can be understood as a weight allocation to stations near the vent, since these will be more sensitive to changes in the source.

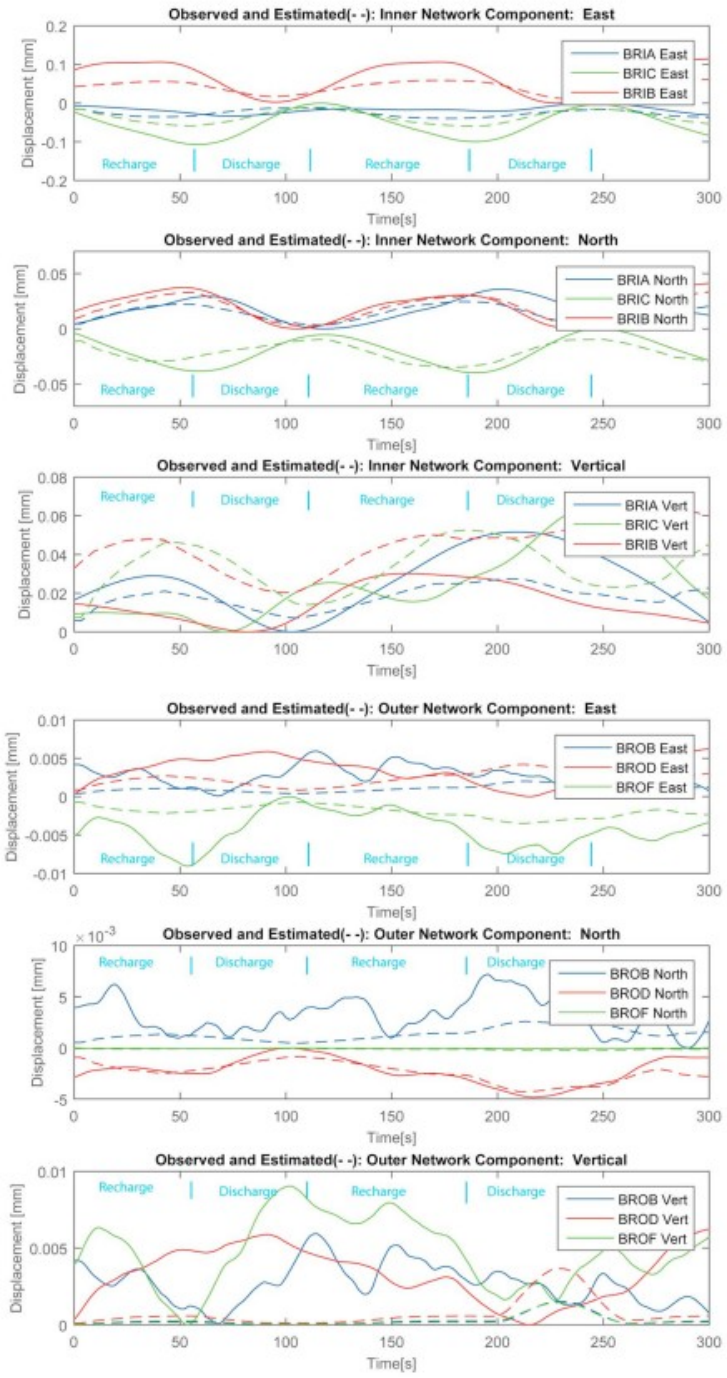

Figure 6. Synthetics and observed time series of displacement for the internal network stations: (a) east, (b) north, and (c) vertical, and for the outer network stations: (d) east, (e) north, and (f) vertical.

Given the proximity of the inner network stations to the geyser, their records are largely insensitive to other sources. These data are well modeled in their horizontal components (Figure 6). However, modeled vertical motions for the inner network differ in shape and magnitude with the exception of BRIA, which is well estimated (see Table S3.4 for misfit residuals). From Figures 2, S1.4, and S1.9 (single-sided amplitude spectrum for the inner network

stations) it can be seen that vertical signals are not dominated by the characteristic cycle of 132 s. Considering that for each station we are estimating two horizontal components that present cyclicity and one vertical component that does not, it is expected that the methodology would better fit horizontal data, as they have more weight in fitting.

The records of the external network are not well fit either (Figure 6), except for the north component of BROD (see Table S3.4 for misfit residuals). There are two reasons for the poor fit of the external network stations. First, the external network may be too far from the vent. Figure S3.2 shows that for a surface radial distance of 15 m, the displacements are less than one third of the maximum values obtained in the area closest to the source. Second, the original and processed records (Figures S1.5–S1.7) do not seem to be influenced by the characteristic cycle of 132 s, which suggests that the stations are not recoding the deformation from the eruptive cycles of the El Jefe geyser (see Figure S1.10 for single-sided amplitude spectrum of outer network stations). Therefore, it is likely that the records of these stations are a superposition of deformation from the El Jefe geyser and other neighboring systems. Figure S1.8 shows a map of the broadband network and the closest active geyser in October 2012. There are active geysers between 20 and 70 m from El Jefe. In addition, Glennon and Pfaff (2003) catalog a series of other geysers that are now inactive around El Jefe, but these may still have subsurface activity.

The sensitivity of the residual to each of the source parameters is explored in Supplement S3 at two randomly chosen times during a cycle (Figure S3.4) by perturbing one parameter and holding the others fixed. The sensitivity of the solutions to changes in the parameters is similar at these times with greatest sensitivity to geometrical parameters (x and y positions, and radius). On the other hand, the pressure is not as well constrained. This indicates that our estimated values for this parameter may not be very accurate. The sensitivity to depth shows that the optimal solution is not necessarily the one that minimizes the global misfit. This is because we impose the additional (geometric) constraint that depth > radius. The McTigue (1987) equations can allow better fits for physically impossible solutions.

To better constrain uncertainties in model parameters (see section S3.4 and Supplement 3), we thus estimated the probability density functions for each parameter at three times (see Figures S3.5–S3.7), generated by 100 sets of data with the addition of random noise. We find uncertainties of about ±0.5 m for the depth, radius, and x,y positions. On the other hand, the pressure shows uncertainties of about ±10 mbar. In general, the distributions are quite narrow reflecting a low level of uncertainty in the best fit model parameters.

5 Discussion

We have found a high correlation between the ground surface displacement, the pressure measurements inside the conduit, and the stages of the

eruptive cycle (see Figures 3 and S1.11). The systematic patterns of ground surface deformation observed in the horizontal components of the inner network are consistent with an increasing pressurization and inflation of the system leading up to an eruption and a faster depressurization and deflation during an eruption. In our modeling, we used this correlation to constrain the source differential pressure, considering hydraulic coupling between a bubble trap and eruption conduit (see section 4, paragraph 5).

The cavity structure found in this study (Figure 4) has similarities to that proposed by Mackenzie (1811) with a large subterranean cavity connected to the ground surface by a conduit with the configuration of an inverted siphon. The subterranean cavity works as a trap for the steam bubbles rising from below. This type of cavity has been proposed for Old Faithful Geyser based on mapping hydrothermal tremor (Vandemeulebrouck et al., 2013, 2014) and video images of horizontal bubble-trap structures in Kamchatka geysers (Belousov et al., 2013), and episodic release of bubbles into geyser conduits in the El Tatio geyser field (Munoz-Saez, Manga, et al., 2015).

The general solution of the problem (Figures 4 and 5) is presented as a time series of the best solution at each considered time, modeled as spherical cavities whose parameters vary spatially and temporally. The deforming region reaches depths of around 10 m, with a lateral extent of about 6 m. Similar cavity dimensions were inferred at other geysers from high-frequency signals produced by hydrothermal tremors generated by cavitating bubbles (Cros et al., 2011; Vandemeulebrouck et al., 2014). The similarity of inferred cavity sizes and locations with these studies is interesting since the methodologies and types of signals are very different.

The shallower solutions appear to define a cylindrical region that we associate with the extension of the geyser conduit down to ~6 m. The deeper solutions identify a second structure toward the north-east, centered at 10 m, that reveals a lateral cavity that apparently is excited during the recharge process. This lateral offset between shallow and deeper solutions supports models with laterally offset cavities.

Results show the activation of a laterally offset cavity at different depths in the two modeled cycles. At the beginning of the first recharge stage (~80 s), a migration of the solution toward the north-east followed by an increase in depth (~110 s) from ~2 to 4 m is observed, accompanied by a pressure drop (see Figure S3.8). This documents a first lateral migration of the source of pressure with a significant depth increase. At the beginning of the second recharge stage (~240 s), a migration of the solution toward the northeast is observed again with a greater increase in radius and depth (reaching a peak at 10 m), and pressure drop (see Figure S3.9). A second lateral migration is accompanied by increase in depth. It can be appreciated that the vertical displacements observed in the internal network (see Figure 6, third panel) are larger in the second modeled cycle, in particular from ~200 s, suggesting that the depth parameter is especially sensitive to vertical displacements.

However, since the vertical signals are not periodic (see Figure S1.10) we cannot correlate vertical signals to periodic variation in depths of the source. Trade-offs between pressure, depth, and radius parameters (Figures S3.3d, S3.3f, and S3.3g) further limit the ability to document the radius and depth and migration of deeper sources.

From the McTigue (1987) equations, the change in pressure is coupled to the radius of the cavity in the term pa^3 in the leading order terms. As noted by Segall (2010), the effects of a finite cavity are sufficiently small that one should consider other approximations (spherical geometry, perfectly elastic behavior, and homogeneous and isotropic response), which may have larger effects. Pressure changes of 4–9 bar during an eruption have been inferred at a geysering well (Rudolph et al., 2012). This is larger than the pressure changes we are estimating (see Figure 5) that are constrained by direct pressure observation inside the conduit (see Figure 3a). As we are assuming hydrostatic behavior for a coupled pressure system, results for the pressure parameter may not be accurate. Also, given the trade-off between parameters, these low-pressure estimates could be compensated with smaller cavities. The strong inter-relationship between cavity size and pressure change provides limits to interpreting subsurface geometry.

The active seismic experiment measured the elastic properties of the medium from the propagation of high-frequency seismic waves (see Supplement S2). From these, a value for the shear modulus of 7.7×10^8 Pa is estimated for the shallowest layer. On the other hand, as discussed in section 4, a shear modulus of $\sim 0.5 \times 10^6$ Pa is required to obtain low-frequency deformations of ~1 mm recorded by broadband sensors over the eruptive cycle. This gives dynamic/static compressibility ratio of around 10^3. This value has been estimated as ~10 for fractured rocks at volcanoes (Gudmundsson, 2011) and is expected to be higher for shallow geyser systems with more prevalent and larger fractures. This reveals relevant analogies between eruptive systems such as volcanoes and those of smaller scales such as geysers, where a very pronounced variation in the elastic modulus is observed for low-frequency deformation compared to seismic values.

6 Summary

The methodology we developed allows us to use long-period deformation to estimate the sources of deformation and their evolution in space and time. We explore, with a modest array of six broadband instruments, the four-dimensional evolution of the subsurface over the full eruption cycle and found some similarities related to tilt signals and frequency-dependent strain response with larger eruptive systems, addressing some of the aspects not understood about geysers (Hurwitz & Manga, 2017).

El Jefe is a highly periodic eruptive system. The cycle can be characterized by two distinct stages: recharge and discharge. The first generates a radial expansion surrounding the geyser, while the second generates contraction.

The temporal behavior of the source correlates strongly with the two main stages of eruption. The cavity structure imaged in this study is consistent with models for geysers composed of an approximately vertical conduit connected to a laterally offset bubble trap.

Perhaps the most relevant result from this study is that the ground surface displacements recorded within a few meters of the geyser vent are correlated with the geyser's eruption cycle and pressure measurements from inside the eruption conduit. Together, this is an unusual set of data that offered an opportunity to connect subsurface and surface measurements in an erupting system.

Acknowledgments

Financial support for this study was provided by FONDAP project 15090013 “Centro de Excelencia en Geotermia de los Andes, CEGA (Andean Geothermal Center of Excellence).” We thank El Tatio team who provided essential help in the laboratory and in the field: Angello Negri, Pablo Ortega, Camilo Sanchez, Sarah Barrett, Max Rudolph, Ameeta Patel, Atsuko Namiki, Chi-Yuen Wang, and Eric King. We also thank Carolina Honores for her help on initial steps of the modelation. The fieldwork was performed with the permission of the Amayras Communities of Caspana and Toconce. A. M. is supported by CONICYT under the grant FONDECYT-3150160. F.O.-C. wishes to thank Proyecto Fondecyt 11140904 (CONICYT). M. M. is supported by NSF 1724986. We also thank Robert Sohn for his comprehensive review of this work. A data set containing the velocity records employed in the modelation can be found in the supporting information. For any support and collaboration, feel free to contact the lead author.

References

Adelstein, E., Tran, A., Saez, C. M., Shteinberg, A., & Manga, M. (2014). Geyser preplay and eruption in a laboratory model with a bubble trap. *Journal of Volcanology and Geothermal Research*, 285, 129– 135. https://doi.org/10.1016/j.jvolgeores.2014.08.005

Belousov, A., Belousova, M., & Nechayev, A. (2013). Video observations inside conduits of erupting geysers in Kamchatka, Russia, and their geological framework: Implications for the geyser mechanism. *Geology*, 41(4), 387– 390. https://doi.org/10.1130/G33366.1

Cros, E., Roux, P., Vandemeulebrouck, J., & Kedar, S. (2011). Locating hydrothermal acoustic sources at Old Faithful Geyser using matched field processing. *Geophysical Journal International*, 187(1), 385– 393. https://doi.org/10.1111/j.1365-246X.2011.05147.x

Cusicanqui, H., Mahon, W. A. J., & Ellis, A. J. (1975). The geochemistry of the El Tatio geothermal field, northern Chile. In second United Nations symposium on the development and utilization of geothermal Resources (pp. 703– 711).

Fernandez-Turiel, J. L., Garcia-Valles, M., Gimeno-Torrente, D., Saavedra-Alonso, J., & Martinez-Manent, S. (2005). The hot spring and geyser sinters of El Tatio, northern Chile. *Sedimentary Geology*, 180(3-4), 125– 147. https://doi.org/10.1016/j.sedgeo.2005.07.005

Fialko, Y., & Simons, M. (2000). Deformation and seismicity in the Coso geothermal area, Inyo County, California: Observations and modeling using satellite radar interferometry. *Journal of Geophysical Research*, 105, 21,781–21,794.

Genco, R., & Ripepe, M. (2010). Inflation-deflation cycles revealed by tilt and seismic records at Stromboli volcano. *Geophysical Research Letters*, 37, L12302. https://doi.org/10.1029/2010GL042925

Giggenbach, W. F. (1978). The isotope composition of waters from the El Tatio geothermal field, northern Chile. *Geochimica et Cosmochimica Acta*, 42(7), 979– 988. https://doi.org/10.1016/0016-7037(78)90287-9

Glennon, J. A., & Pfaff, R. M. (2003). The extraordinary thermal activity of El Tatio Geyser Field, Antofagasta region, Chile. GOSA Trans. 8, 31– 78.

Gudmundsson, A. (2011). *Rock fractures in geological processes*. Cambridge: Cambridge University Press. https://doi.org/10.1017/CBO9780511975684

Hurwitz, S., & Manga, M. (2017). The fascinating and complex dynamics of geyser eruptions. *Annual Review of Earth and Planetary Sciences*, 45(1), 31–59. https://doi.org/10.1146/annurev-earth-063016-015605

Hurwitz, S., Sohn, R. A., Luttrell, K., & Manga, M. (2014). Triggering and modulation of geyser eruptions in Yellowstone National Park by earthquakes, earth tides, and weather. *Journal of Geophysical Research: Solid Earth*, 119, 1718– 1737. https://doi.org/10.1002/2013JB010803

Hutchinson, R. A. (1985). Hydrothermal changes in the upper geyser basin, Yellowstone National Park, after the 1983 Borah Peak, Idaho, earthquake. In Proceedings of Workshop (Vol. 28, pp. 612– 624).

Hutchinson, R. A., Westphal, J. A., & Kieffer, S. W. (1997). In situ observations of Old Faithful Geyser. *Geology*, 25(10), 875– 878. https://doi.org/10.1130/0091-7613(1997)025<0875:ISOOOF>2.3.CO;2

Ingebritsen, S. E., & Rojstaczer, S. A. (1993). Controls on geyser periodicity. *Science*, 262(5135), 889– 892. https://doi.org/10.1126/science.262.5135.889

Johnson, S. H. (1976). Interpretation of split-spread refraction data in terms of plane dipping layers. *Geophysics*, 41(3), 418– 424. https://doi.org/10.1190/1.1440623

Karlstrom, L., Hurwitz, S., Sohn, R., Vandemeulebrouck, J., Murphy, F., Rudolph, M. L., Johnson, M. S., Manga, M., & McCleskey, R. B. (2013). Eruptions at Lone Star Geyser, Yellowstone National Park, USA: 1. Energetics and eruption dynamics. *Journal of Geophysical Research: Solid Earth*, 118, 4048– 4062. https://doi.org/10.1002/jgrb.50251

Kedar, S., Kanamori, H., & Sturtevant, B. (1996). The origin of harmonic tremor at Old Faithful Geyser. *Nature*, 379(6567), 708– 711. https://doi.org/10.1038/379708a0

Kedar, S., Kanamori, H., & Sturtevant, B. (1998). Bubble collapse as the source of tremor at Old Faithful Geyser. *Journal of Geophysical Research*, 103(B10), 24,283– 24,299. https://doi.org/10.1029/98JB01824

Kieffer, S. W. (1984). Seismicity at Old Faithful Geyser: An isolated source of geothermal noise and possible analogue of volcanic seismicity. *Journal of Volcanology and Geothermal Research*, 22, 59– 95. https://doi.org/10.1016/0377-0273(84)90035-0

Lynne, B. Y., Heasler, H., Jaworowski, C., Foley, D., Smith, I. J., & Smith, G. J. (2018). Ground penetrating radar documents short-term near-surface hydrological changes around Old Faithful Geyser, Yellowstone National Park, USA. *Journal of Volcanology and Geothermal Research*, 354, 1– 12. https://doi.org/10.1016/j.jvolgeores.2018.01.018

Lynne, B. Y., Heasler, H., Jaworowski, C., Foley, D., Smith, I. J., Smith, G. J., & Sahdarani, D. (2017). Using ground penetrating radar, scanning electron microscopy and thermal infrared imagery to document near-surface hydrological changes in the Old Faithful Geyser area, Yellowstone National Park, USA. *Geothermics*, 68, 33– 53. https://doi.org/10.1016/j.geothermics.2017.02.007

Lyons, J. J., Waite, G. P., Ichihara, M., & Lees, J. M. (2012). Tilt prior to explosions and the effect of topography on ultra-long-period seismic records at Fuego volcano, Guatemala. *Geophysical Research Letters*, 39, L08305. https://doi.org/10.1029/2012GL051184

Mackenzie, G. (1811). *Travels in the Island of Iceland, Edinburgh* (Vol. 27). Edinburgh: Alam and Company.

Maeda, Y., & Takeo, M. (2011). Very-long-period pulses at Asama volcano, central Japan, inferred from dense seismic observations. *Geophysical Journal International*, 185(1), 265– 282. https://doi.org/10.1111/j.1365-246X.2011.04938.x.

Marinovic, N., & Lahsen, A. (1984). *Hoja Calama: región de Antofagasta: carta geológica de Chile 1: 250.000*. Chile: Servicio Nacional de Geología y Minería.

McTigue, D. F. (1987). Elastic stress and deformation near a finite spherical magma body: Resolution of the point source paradox. *Journal of Geophysical Research*, 92, 12,931– 12,940. https://doi.org/10.1029/JB092iB12p12931

Munoz-Saez, C., Manga, M., & Hurwitz, S. (2018). Hydrothermal discharge from the El Tatio basin, Atacama, Chile. *Journal of Volcanology and Geothermal Research*, 361, 25– 35. https://doi.org/10.1016/j.jvolgeores.2018.07.007

Munoz-Saez, C., Manga, M., Hurwitz, S., Rudolph, M. L., Namiki, A., & Wang, C. Y. (2015). Dynamics within geyser conduits, and sensitivity to environmental perturbations: Insights from a periodic geyser in the El Tatio geyser field, Atacama Desert, Chile. *Journal of Volcanology and Geothermal Research*, 292, 41– 55. https://doi.org/10.1016/j.jvolgeores.2015.01.002

Munoz-Saez, C., Namiki, A., & Manga, M. (2015). Geyser eruption intervals and interactions: Examples from el Tatio, Atacama, Chile. *Journal of Geophysical Research: Solid Earth*, 120, 7490– 7507. https://doi.org/10.1002/2015JB012364

Munoz-Saez, C., Saltiel, S., Manga, M., Nguyen, C., & Gonnermann, H. (2016). Physical and hydraulic properties of modern sinter deposits: El Tatio, Atacama. *Journal of Volcanology and Geothermal Research*, 325, 156– 168. https://doi.org/10.1016/j.jvolgeores.2016.06.026

Namiki, A., Ueno, Y., Hurwitz, S., Manga, M., Munoz-Saez, C., & Murphy, F. (2016). An experimental study of the role of subsurface plumbing on geothermal discharge. *Geochemistry, Geophysics, Geosystems*, 17, 3691– 3716. https://doi.org/10.1002/2016GC006472

National Acedemies of Science, Engineering and Medicine (2017). *Volcanic Eruptions and their Repose, Unrest, Precursors, and Timing*. Washington, DC: The National Academies Press. https://doi.org/10.17226/24650

Nicolau, C., Reich, M., & Lynne, B. (2014). Physico-chemical and environmental controls on siliceous sinter formation at the high-altitude El Tatio geothermal field, Chile. *Journal of Volcanology and Geothermal Research*, 282, 60– 76. https://doi.org/10.1016/j.jvolgeores.2014.06.012

Nishimura, T., Ichihara, M., & Ueki, S. (2006). Investigation of the Onikobe geyser, NE Japan, by observing the ground tilt and flow parameters. *Earth, Planets and Space*, 58(6), e21– e24. https://doi.org/10.1186/BF03351967

Pillet, R., & Virieux, J. (2007). The effects of seismic rotations on inertial sensors. *Geophysical Journal International*, 171(3), 1314– 1323. https://doi.org/10.1111/j.1365-246X.2007.03617.x

Rodgers, P. W. (1968). The response of the horizontal pendulum seismometer to Rayleigh and love waves, tilt, and free oscillations of the Earth. *Bulletin of the Seismological Society of America*, 58(5), 1385– 1406.

Rudolph, M. L., Manga, M., Hurwitz, S., Johnston, M., Karlstrom, L., & Wang, C. Y. (2012). Mechanics of Old Faithful Geyser, Calistoga, California. *Geophysical Research Letters*, 39, L24308. https://doi.org/10.1029/2012GL054012

Rudolph, M. L., & Sohn, R. A. (2017). A model for internal oscillations in geysers, with application to Old Faithful (Yellowstone, USA). *Journal of Volcanology and Geothermal Research*, 343, 17– 24. https://doi.org/10.1016/j.jvolgeores.2017.04.023

Sanderson, R. W., Johnson, J. B., & Lees, J. M. (2010). Ultra-long period seismic signals and cyclic deflation coincident with eruptions at Santiaguito volcano, Guatemala. *Journal of Volcanology and Geothermal Research*, 198(1–2), 35– 44. https://doi.org/10.1016/j.jvolgeores.2010.08.007

Segall, P. (2010). *Earthquake and volcano deformation*. Princeton, NJ: Princeton University Press. https://doi.org/10.1515/9781400833856

Steinberg, G. S., Merzhanov, A. G., & Steinberg, A. S. (1981). Geyser process: Its theory, modeling, and field experiment, Part 1, theory of the Geyser process. *Modern Geology*, 8, 67– 70.

Tassi, F., Aguilera, F., Darrah, T., Vaselli, O., Capaccioni, B., Poreda, R. J., & Huertas, A. D. (2010). Fluid geochemistry of hydrothermal systems in the Arica-Parinacota, Tarapacá and Antofagasta regions (northern Chile). *Journal of Volcanology and Geothermal Research*, 192(1–2), 1– 15. https://doi.org/10.1016/j.jvolgeores.2010.02.006

Vandemeulebrouck, J., Roux, P., & Cros, E. (2013). The plumbing of Old Faithful Geyser revealed by hydrothermal tremor. *Geophysical Research Letters*, 40, 1989– 1993. https://doi.org/10.1002/grl.50422

Vandemeulebrouck, J., Sohn, R. A., Rudolph, M. L., Hurwitz, S., Manga, M., Johnston, M. J., Soule, S. A., McPhree, D., Glen, J. M., Karlstrom, L., & Murphy, F. (2014). Eruptions at Lone Star Geyser, Yellowstone National Park, USA: 2. Constraints on subsurface dynamics. *Journal of Geophysical Research: Solid Earth*, 119, 8688– 8707. https://doi.org/10.1002/2014JB011526

Waite, G. P., Nadeau, P. A., & Lyons, J. J. (2013). Variability in eruption style and associated very long period events at Fuego volcano, Guatemala. *Journal of Geophysical Research: Solid Earth*, 118, 1526– 1533. https://doi.org/10.1002/jgrb.50075

Walter, T. R., Jousset, P., Allahbakhshi, M., Witt, T., Gudmundsson, M. T., & Hersir, G. P. (2018). Underwater and drone based photogrammetry reveals structural control at Geysir geothermal field in Iceland. *Journal of Volcanology and Geothermal Research*. https://doi.org/10.1016/j.jvolgeores.2018.01.010